IAC–18–C4.6.2.x47764

Chemical Propulsion System Design for a 16U Interplanetary CubeSat

Karthik Venkatesh Mani
Politecnico di Milano, Italy
karthikvenkatesh.mani@polimi.it

Francesco Topputo
Politecnico di Milano, Italy
francesco.topputo@polimi.it

Angelo Cervone
Delft University of Technology, the Netherlands
a.cervone@tudelft.nl

Stand-alone interplanetary CubeSats to Mars require primary propulsion systems for orbit manoeuvring and trajectory control. The context is a 30 kg 16U Interplanetary CubeSat mission on a hybrid high-thrust & low-thrust trajectory utilising a Dual Chemical-Electric Propulsion System to achieve Earth escape (high-thrust) and perform autonomous deep-space cruise (low-thrust) to Mars. Mission analysis is performed to estimate the required ΔV ($\sim 445\,\mathrm{m/s}$) for Earth escape and Mars circularisation, and calculate the required thrusts and burn durations while minimising gravity losses, Van Allen belt crossings, and irrecoverable destabilisation. Design of an ADN-based monopropellant thruster and an Ethanol-H_2O_2 based bipropellant thruster are performed and the critical design details regarding propellant characteristics, system sizes, operating pressures, material selection and geometry of feed systems, thrust chambers, and nozzles are delineated. Performances analysis of the monopropellant thruster yields a maximum thrust of 3.18 N (two thrusters with 1.54 N each) and an $I_{sp} = 259.7$ s with nozzle area ratio of 100. Similarly, the bipropellant thruster yields a thrust of 2.91 N and an $I_{sp} = 303.15$ s. The overall mass and volume of the monopropellant system are 5.6 kg (18.7%) and 7U, respectively. The bipropellant system weighs 4.85 kg (16.17%) while occupying 6.5U space.

1. Introduction

CubeSats have been used for Earth observation missions since early 2000s with multiple applications such as climate assessment, biological research, atmospheric characterisation etc. [1]. CubeSat design and mission development have been primarily pursued by universities and small-spacecraft consortia and there is a growing interest among national and international space organisations. Contemporary CubeSats operate at Low-Earth Orbits (LEOs) and their size range is 1U to 6U while larger form factors are under development [2]. Earth-based CubeSats are designed to maximise payload performance and do not have primary propulsion systems for orbital manoeuvring since such operations are not considered critical. Very few CubeSat missions have performed a technology demonstration of propulsion systems, albeit with limited capability. The IMPACT mission utilised multiple electrospray thrusters developed by MIT and the BricSAT-P mission utilised μCathode Arc Thrusters by George Washington University [3]. The propulsion systems utilised in present-day CubeSats are for attitude control, station-keeping, and reaction wheel desaturation [4].

Interplanetary CubeSat missions expand the horizon of CubeSat applications and enable Solar System exploration at a high science-to-investment ratio. Mission applications include Mars science observation [5], Mars communication relay and network setup [6, 7], asteroid mineral mapping, heliophysics studies [8], lunar meteoroid observation [2] etc. Improvements in critical fields like long-distance communication, deep-space autonomous guidance-navigation-control, propulsion for trajectory control, accurate ADCS, and high-speed low-power on-board data processing are required [8].

CubeSat missions to Mars could be achieved through a) in-situ deployment by a mothership and b) highly flexible stand-alone CubeSats on deep-space cruise [9]. The Mars Cube One (MarCO) mission, designed by JPL and launched alongside InSight lander mission in May 2018, is the only interplanetary CubeSat in existence [6, 10]. The mission is injected directly into the interplanetary space by the launcher. MarCO mission utilises two 6U CubeSats that shall

perform a Mars flyby and provide communication relay and support during InSight's Mars atmospheric entry. The CubeSats use Vacco MiPS (Micro CubeSat Propulsion System) for executing two trajectory control manoeuvres [11]. Stand-alone CubeSat missions to Near-Earth Objects have been shown to be feasible, such as M-ARGO mission by ESA [12].

The stand-alone interplanetary CubeSat mission under consideration in this work is the **M**ars **A**tmospheric **R**adiation **I**maging **O**rbiter (MARIO) mission. It is envisaged to be launched into the Supersynchronous Geostationary Transfer Orbit (SSGTO), execute orbit raising and Earth escape, perform a low-thrust interplanetary transfer, achieve ballistic capture at Mars, and then enter an areosynchronous orbit. Launch windows could be broadened and the launch could be shared with any primary payload that is bound for such a high-energy Earth orbit. Additionally, such launches have a higher frequency (∼10/year) compared to direct heliocentric orbit launches (∼2/year).

Robust primary propulsion systems become indispensable for interplanetary missions since precise trajectory control and major orbital manoeuvre operations are required. Mani et al [9] have delineated the characteristics of the the dual chemical-electric propulsion systems design that is utilised in the MARIO mission to execute a hybrid high-thrust & low-thrust trajectory. The motivation is to develop robust, compact, and powerful primary propulsion systems that shall enable such interplanetary missions and increase the mission flexibility and autonomy. This work focuses on the chemical propulsion system which is used in the high-thrust stage to perform orbit raising manoeuvres and achieve a swift Earth escape to reduce the residence time in the Van Allen radiation belts and consequently avoid radiation damage. The chemical propulsion system is also utilised in performing a manoeuvre at Mars orbit to initiate the circularisation towards an areosynchronous orbit.

Chemical propulsion systems applicable to interplanetary CubeSats include monopropellant thrusters [13, 14], bipropellant thrusters [15], tripropellant [16], cold gas [17, 3, 10], warm gas [18], solid [19] and hybrid motor systems [20]. These systems have been manufactured and tested on-board large satellites but they face multiple issues over miniaturisation [21]. The monopropellant and bipropellant systems are the most suitable for stand-alone interplanetary CubeSat wanting to achieve Earth escape due to their superior performance characteristics [17].

In this work, the mission characteristics are highlighted in section 2. The chemical propulsion design strategy is elucidated in section 3 and the design characteristics and performances of monopropellant and bipropellant systems are discussed in section 4 and section 5, respectively. These sections highlight the propellant properties, feed system design, thrust chamber & nozzle design and their corresponding performance values relating to thrust, specific impulse, velocities etc.

2. Mission Characteristics

The key phases of the MARIO mission are a) orbit raising & Earth escape, b) deep-space autonomous cruise, c) ballistic capture and d) areosychronous orbit emplacement. The high-thrust chemical propulsion system is utilised in the first phase to provide the necessary ΔV for Earth escape. The spacecraft is inserted into a highly elliptical super synchronous geostationary transfer orbit with a perigee of 295 km and an apogee of 90,000 km, which is used for some communication satellite launches. For instance, SpaceX's Falcon 9 v1.1 rocket launched Thaicom 6* in January 2014 in that orbit. Since the launch frequency of such communication satellites is higher than Earth escape missions, the selection of this initial orbit improves the launch opportunities. Additionally, owing to the high eccentricity of the orbit, the necessary escape velocity at the perigee is significantly low. The orbit raising manoeuvres are illustrated in Fig. 1.

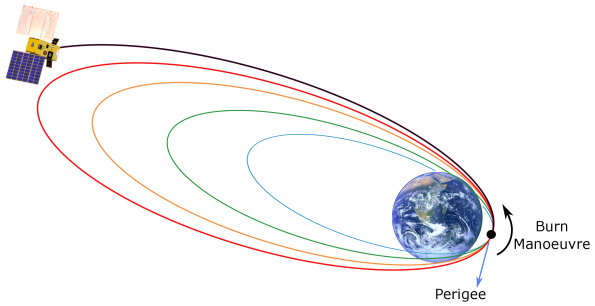

Fig. 1: Illustration of orbit raising manoeuvres and Earth escape

High thrust is used in this phase primarily due to the presence of Van Allen radiation belts and the expected multiple crossings of the spacecraft through

*SpaceX Falcon 9 Data Sheet - Space Launch Report http://www.spacelaunchreport.com/falcon9ft.html

these. Thus, it is essential to achieve a swift escape and reduce the radiation damage. A low thrust option will lead to excessive radiation damage due to a significantly high residence time of the spacecraft in the radiation belts.

The chemical propulsion system is necessary to provide the required ΔV within a short duration. Owing to the size and mass of the spacecraft, 16U and ∼30 kg, there is a limitation on maximum thrust since very high thrusts, in tandem with thrust misalignment and engine misfire, might lead to irrecoverable destabilitsation. Additionally, lower thrust values lead to longer thruster burn times, which results in higher gravity losses. Thus, the propulsion system needs to fire for a specific duration, in terms of burn time or burn arc about the perigee, and with a specific thrust such that Earth escape is achieved swiftly while destabilisation, gravity losses, and radiation accumulation are reduced.

The initial insertion orbit semi-major axis, eccentricity, inclination, right-ascension of the ascending node, argument of perigee, and true anomaly are $[a, e, i, \Omega, \omega, \theta] = [51526 \text{ km}, 0.8705, 0.01°, 0°, 0°, 0°]$. The perigee altitude is 295 km and the apogee altitude is 90,000 km. The perigee velocity of the initial launch orbit is 10.57 km/s and the escape velocity at perigee point is 10.93 km/s. Thus, the ΔV for escape, at the perigee point considering an impulsive manoeuvre, is $\sim$ 360 m/s.

2.1 Orbit raising manoeuvre strategies

Earth escape is achieved by executing multiple orbit raising manoeuvres using the chemical propulsion system. Since real manoeuvres are considered, the thruster has to burn for a specific duration in each orbit. A single burn manoeuvre to achieve escape would drastically increase the gravity losses. Thus, the burns must be split prudently such that swift escape is achieved while gravity losses are controlled. The two strategies to execute the burn manoeuvres are a) constant burn time and b) constant burn arc. In the first strategy, a thrust (T) & burn time (t_b) combination that enables the fastest escape while considering the system constraints is determined and in the second strategy, a thrust & burn arc ($\Delta\theta_b$) combination is determined. These strategies help us size and design the chemical propulsion system in accordance with the mission operations.

The execution of the burn is split equally such that it is initiated at $t_b/2$ or $\Delta\theta_b/2$ before the perigee and it is completed at $t_b/2$ or $\Delta\theta_b/2$ after the perigee, as illustrated in Fig.2. This enables a more efficient throttling manoeuvre and reduces gravity losses.

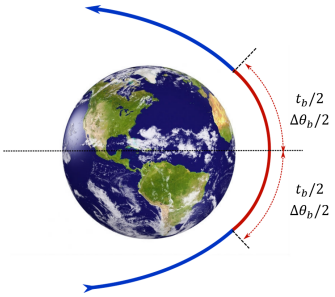

Fig. 2: Burn strategy with equal splitting of t_b and $\Delta\theta_b$ about Perigee. The powered trajectory is red and the ballistic trajectory is blue.

To calculate the spacecraft trajectory for the constant burntime approach, a 2-body problem is assumed and the injection orbit parameters are initialised in the beginning. The goal of the trajectory analysis is to find two things, a) the thrust-burntime combination for the lowest flight time to escape and b) the required total ΔV and the corresponding propellant mass spent in achieving that escape.

Different thrust-burntime combinations are sampled to find the $T - t_b$ combination that yields the lowest transfer time. Thus, a nested loop containing a range of thrusts and a range of burntimes is utilised. Within this nested loop, the procedure to calculate the trajectory is implemented. In the constant burntime approach, the Mean anomaly is calculated using the given burntime and the corresponding Eccentric anomaly is obtained. The true anomaly at which the burn is executed is calculated using Eq. (1)

$$\theta_{pb} = -2\tan^{-1}\left[\sqrt{\frac{1+e_{pb}}{1-e_{pb}}}\,\tan\left(\frac{E_{pb}}{2}\right)\right] \tag{1}$$

The subscript 'pb' indicates pre-burn values. The true anomaly is denoted by θ, eccentricity is e, and the Eccentric anomaly is E. The Keplerian orbital elements before the burn are then converted to Cartesian coordinates. The orbital equation of motion is integrated over the burntime to obtain the burn trajectory.

$$\ddot{r} + \frac{\mu}{r^3}\hat{r} = \frac{\vec{T}}{m} \tag{2}$$

$$\dot{m} = -\frac{\left|\vec{T}\right|}{I_{sp}\, g_0} \tag{3}$$

$$\vec{T} = F \cdot T_{max} \cdot \frac{\vec{v}}{||\vec{v}||} \tag{4}$$

Here r is the distance, μ is the gravitational parameter of Earth, m is the mass, $\vec{T}$ is the thrust vector, $\vec{v}$ is the instantaneous velocity vector, F is the throttle, and T_{max} is the magnitude of maximum thrust. Once the burn trajectory is calculated, the orbital elements at the end of the burn and for the next manoeuvre are calculated. The ballistic flight time is calculated using the eccentric anomalies E_{ab} and E_{nm}, where 'ab' and 'nm' indicate after-burn and new-manoeuvre, respectively. The ballistic flight trajectory is calculated by integrating the equations of motion over the ballistic flight time, however while setting the thrust to zero.

The procedure to integrate the powered and ballistic trajectories is done until Earth escape is achieved. The total transfer time is calculated by summing up the burn and ballistic durations of each orbit until escape. Depending upon the thrust and burntime, the total transfer time and the number of manoeuvres vary. In addition to this, the burn arc varies for each burn since the orbital geometry varies but the burntime is kept constant. The combination that yields the lowest flight time to escape Earth and the lowest number of manoeuvres while adhering to the system constraints is selected.

In the constant burn arc strategy, the $\Delta\theta_b$ is set for each manoeuvre. The burn commences at $-\Delta\theta_b/2$ and ends at $+\Delta\theta_b/2$ from the point of perigee. The time between them is calculated and the burn trajectory is obtained by integrating the equation of motion with T as an input. A series of thrusts and burn arcs are sampled and the $T-\Delta\theta_b$ combination that yields the lowest transfer time for Earth escape is selected. The burntime varies for each manoeuvre since $\Delta\theta_b$ is held constant.

For the constant burntime and constant burn arc strategies, the overall propellant mass m_p is calculated by subtracting the final state m_f from the initial mass m_0. The overall ΔV is calculated using the Tsiolkovsky's rocket equation (Eq. (5))

$$\Delta V = I_{sp}\, g_0\, \log\left[\frac{m_0}{m_f}\right] \tag{5}$$

These parameters, along with the $T - t_b$ and $T - \Delta\theta_b$ values, govern the chemical propulsion system design.

2.2 Circularisation burn at Mars

The chemical propulsion system is utilised not only for Earth escape but also in the circularisation manoeuvre at Mars. Once the Earth escape is achieved, the chemical propulsion system is shut off and the low-thrust electric propulsion system starts firing to enable the heliocentric transfer to Mars [9]. The spacecraft executes a long duration electric propulsion burn to reach Mars and enters a Martian orbit through *Ballistic capture*[22].

The capture is achieved solely by natural gravitational forces and it can also escape using the same mechanism. Additionally, the ballistic capture orbit has a very high eccentricity and it is unsuitable for scientific observation missions. Thus, circularisation to an areosynchronous orbit needs to be done. Performing the circularisation manoeuvre using only the low-thrust electric propulsion leads to an extremely long operational time. Thus, to expedite the circularisation, the chemical propulsion system is utilised to provide a small ΔV ($\sim 45\,\mathrm{m/s}$) to reduce the eccentricity and then the electric propulsion system is utilised to complete the operation.

3. System Design Strategy

3.1 Requirements

The primary requirements for the chemical propulsion system for the MARIO mission that are established pertain to maximum thrust, ΔV, maximum burn duration, mass and safety. The propulsion system requirements are listed in Tab. 1

Tab. 1: Chemical Propulsion System Requirements

ID	Type	Requirement
CPROP-01	PER	The chemical propulsion system shall provide a minimum **ΔV = 445 m/s** for orbital transfer and circulatisation manoeuvres.
CPROP-02	PER	The chemical propulsion system shall have a maximum thrust of **3 N**
CPROP-03	PER	The maximum thrusting time of the chemical propulsion system shall be **600 seconds** per orbital manoeuvre
CPROP-04	CON	The total mass of the chemical propulsion system shall be no more than **7.5 kg**.
CPROP-05	CON	The chemical propulsion system shall utilise non-toxic propellants

The rationale for CPROP-01 comes from the ΔVs required for Earth escape and circularisation at Mars.

The initial orbit has a perigee altitude of 295 km and an apogee altitude of 90,000 km. The perigee velocity at the initial orbit is 10.5761 km/s and the required escape velocity at that perigee altitude is 10.9358 km/s. Thus, in the ideal case without losses, the ΔV required for escape is ∼360 m/s. A 10% margin is considered to include for gravity losses and other miscellaneous operational errors, thereby yielding a margined ΔV_{esc} of 396 m/s.

To expedite the circularisation operation at Mars to an areostationary orbit from an initial high eccentricity ballistic capture orbit, a deceleration manoeuvre at the periareion is executed. The deceleration manoeuvre requires a ΔV of 45 m/s [23]. An additional ∼10% margin is placed and the ΔV_{circ} is calculated to be 49 m/s. Thus, the overall minimum ΔV_{tot} that is required to be provided by the chemical propulsion system is set at 396 + 49 = 445 m/s.

Requirement CPROP-02 establishes a limitation on thrust and CPROP-03 establishes the maximum burn time. For a 30 kg spacecraft, the combination of maximum thrust and burn durations are set to effectively distribute the ΔV required to escape Earth into multiple manoeuvres and to reduce the overall transfer time while keeping the gravity loss in control. In contrast, a single burn manoeuvre to escape leads to a gravity loss of ∼23%. Additionally, the limitations on thrust and burntime lead to the avoidance of irrecoverable destabilisation and excessive heat build up. Considering a 1 mm misalignment, the torque is 3 mNm and the momentum is 1.8 Nms. Simultaneous thrust vectoring and reaction wheel operation are essential for controlling the momentum build-up and proper directional firing. The maximum mass requirement, CPROP-04, is capped at 25% of the overall spacecraft mass. The CubeSat is assumed to be a secondary payload and non-toxic propellants need to be used to avoid any damage to the primary spacecraft as well as any self-damage. The toxic propellants require rigorous containment strategies that increase the system cost. This requirement can be relaxed if the propellant has a low-toxicity and affordable control measures can be implemented.

3.2 System types

The types of chemical propulsion system under consideration are solid, liquid, and cold gas. The key design driver is the specific impulse, I_{sp}, which is the highest for liquid thrusters and lowest for cold gas thrusters. In addition to this, the cold gas thrusters for cubesats do not satisfy requirements on minimum thrust (< 1 N), which lead to very long flight times, and maximum mass (> 8 kg). The solid thrusters have a lower I_{sp} than liquid thrusters but are able to provide a higher thrust. However, since multiple manoeuvres are required, *start-stop* capability is indispensable for the chemical propulsion system. Thus, the choice of the propulsion type is liquid propulsion.

In liquid chemical propulsion systems, the specific impulse could vary between 200 s to 350 s, depending upon the type of the propellants. Two propulsion system types are considered: Monopropellant thrusters and Bipropellant thrusters. The monopropellant thrusters that use ammonium dinitramide (ADN) blends are considered since they satisfy the non-toxicity requirement (CPROP-05) and have high density. The specific impulse of the monopropellant system is 260 seconds and an ADN-based monopropellant system has been successfully demonstrated in space[24, 25]. The bipropellant thrusters that utilise hydrogen peroxide (H_2O_2) and ethanol (C_2H_5OH) also satisfy CPROP-05. The specific impulse of such bipropellant thrusters is 315 s [15].

3.3 Design procedure

The design procedure involves the selection of thrust and burn durations for both the monopropellant and bipropellant thrusters. This is based on a parametric analysis to calculate the trajectory, the total time for Earth escape through orbit raising, and the required propellant mass for the operations (see section 2.1). Depending on the I_{sp}, the total flight time, propellant mass and consequently the thrust and burn durations vary[†]. The propulsion system sizing is done using the mission requirements, the system requirements and system type. Propellant characteristics are analysed and the feed system is designed. The thrust chamber and nozzle design take into account the combustion properties and performance requirements.

4. Monopropellant thruster

The parametric analysis to calculate the thrust and burn duration values based on minimum transfer time to escape Earth is performed. The monopropellant I_{sp} is set at 260 seconds while the minimum and maximum thrust values are set at 2N and 3N, respectively. For the constant burntime strategy, the sampled values of t_b range from 400 to 600 seconds. For the constant burnarc strategy, the sampled values of $\Delta\theta_b$ range from 35° to 55° of total arc. To find

[†]All thrust and specific impulse values used in this work pertain to vacuum condition

the precise thrust and burn duration, 1000 values of thrust, t_b and $\Delta\theta_b$ are sampled.

The total transfer time or the total Earth orbiting time as a function of T and t_b is illustrated in Fig. 3a for the constant burntime strategy. The $T-t_b$ combination is picked from the zone where the transfer time is the lowest (top-right, dark blue). Some combinations yield a transfer time that is greater than 150 days (3600 hours) and they are discarded because a swift transfer is desired. Similarly, Fig. 3b illustrates the total transfer time as a function of T and $\Delta\theta_b$ (burn arc).

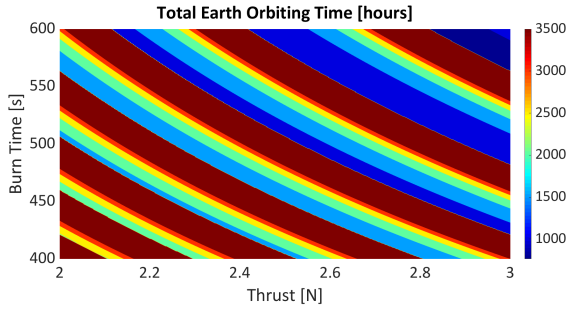

(a) Transfer time (hr) for constant t_b strategy

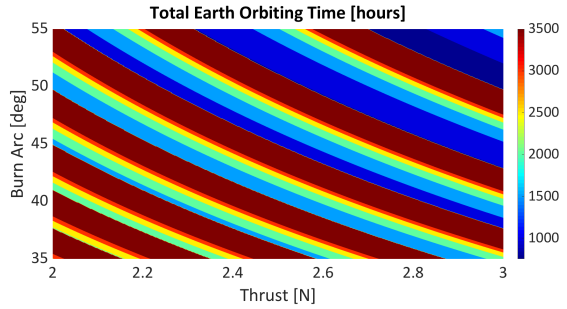

(b) Transfer time (hr) for constant $\Delta\theta_b$ strategy

Fig. 3: Transfer time (hr) as a function of T & t_b and T & $\Delta\theta_b$ for $I_{sp} = 260$ s

If the burntime is kept constant for each manoeuvre, the thrust $T = 2.87$ N, burntime $t_b = 589.5792$ s, and the lowest total transfer time $P = 764.65$ hours. The maximum and minimum burn arcs corresponding to this t_b are 53.19° and 52°. If the burn arc is set constant for each manoeuvre, $T = 2.77$ N, $\Delta\theta_b = 53.67°$ and the lowest transfer time $P = 757.92$ hours. The maximum burntime corresponding to this $\Delta\theta_b$ is 611.3 seconds, which violates CPROP-03, albeit by a small amount.

These parameters indicate the thrust that needs to be provided and the burn durations for which each manoeuvre should be executed to achieve the lowest transfer time. However, the design of thruster cannot be done precisely for this thrust and some margins and contingency measures need to be taken. Thus, the thruster is designed for a thrust of 3 N and a robust control authority can then be provided to the thruster to execute such precise manoeuvres. Thruster firing at 3 N reduces the t_b for each manoeuvre by ∼4.5% and the transfer time increases by $< 1\%$. Similarly, the $\Delta\theta_b$ for each manoeuvre reduces by 7.3% and the corresponding transfer time increases by $< 1\%$.

The constant burntime strategy using monopropellant thrusters firing at $T = 2.87$ N for $t_b = 589.57$ seconds yields a total $\Delta V = 363.041$ m/s and a propellant mass $m_p = 3.96$ kg. The ideal ΔV for escape at perigee while considering impulsive manoeuvres is 359.66 m/s. Thus, the difference between the ΔVs of real and ideal manoeuvres is 3.38 m/s, which is ∼1% higher than the ideal one. The constant burn arc strategy using the thrusters firing at $T = 2.77$ N for a $\Delta\theta_b = 53.67°$ yields a total $\Delta V = 363.29$ m/s and a propellant mass $m_p = 3.96$ kg. This extra ΔV accounts for the gravity losses accumulated over multiple manoeuvres and it is well within the applied margin of 10%. The propellant mass ($m_{p,mg}$) pertaining to the margined value ($\Delta V_{mg} = 396$ m/s) is 4.32 kg. Another 0.38 kg of propellant mass is added to accommodate the Mars circularisation $\Delta V_{circ,mg} = 49$ m/s. Both strategies lead to an escape after the 6^{th} orbit, bringing the total number of Van Allen belt crossings to 13 (12 elliptical crossings plus 1 parabolic crossing). The orbital transfer is illustrated in Fig. 4

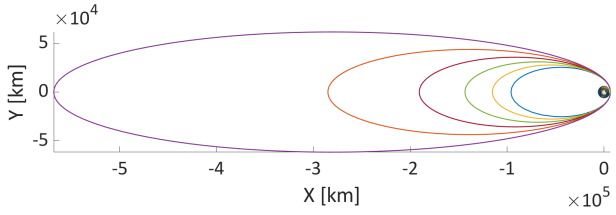

Fig. 4: Orbit raising using monopropellant thrusters with constant t_b strategy

To provide the necessary thrust, either a single 3N thruster or two 1.5N thrusters can be utilised. ADN-based thrusters providing 1 - 1.5N thrust are currently under development [25, 26]. Thus, this analysis considers two 1.5N thrusters to provide the necessary maximum thrust. The mission parameters are listed in Tab. 2

Tab. 2: Orbit raising parameters using monopropellant thruster with constant t_b strategy

Parameter	Value
Initial Mass, m_i	30 kg
Required Thrust, T	2.87 N
Specific Impulse, I_{sp}	260 s
Burn Time per manoeuvre, t_b	589.58 s
Orbit raising manoeuvres	6
Ideal ΔV	359.66 m/s
Real ΔV	363.041 m/s
Margined ΔV (10% margin)	396 m/s
Propellant mass (real), m_p	3.96 kg
Propellant mass (margined), $m_{p,mg}$	4.32 kg
Final mass at Earth escape, $m_{f,esc}$	26.04 kg
Mars circularisation ΔV_{circ}	45 m/s
Margined $\Delta V_{circ,mg}$ ($\sim$10% margin)	49 m/s
Propellant mass for $\Delta V_{circ,mg}$	0.38 kg
Final mass at Mars, $m_{f,circ}$	19.31 kg[1]
Overall propellant mass, $m_{p,mg,ovr}$	4.7 kg

[1] After low-thrust transfer to Mars and chemical circularisation manoeuvre

4.1 Propellant properties

The propellant considered is an ammonium dinatramide (ADN),$NH_4[N(NO_2)_2]$, blend propellant - FLP-106 with a liquid phase density of 1357 kg/m^3 at 25°C. ADN is a solid white salt with ammonia cation (NH_{4^+}) and dinitramide anion ($N(NO_2)_{2^-}$) which is readily soluble in water and other polar solvents. FLP-106 consists of 64.6% ADN, 23.9 % water and 11.5% low-volatile fuel [27]. In comparison, the widely used monopropellant Hydrazine has a density of 1.004 kg/m^3 at room temperature and has a very high toxicity. At nozzle expansion ratio of 50, the FLP-106 propellant can yield an $I_{sp} \approx 260$ s [28]. Some key properties of FLP-106 are listed in Tab. 3 [27, 28].

Tab. 3: FLP-106 liquid monopropellant properties

Property	Value
Molecular mass, $\mathfrak{M}$	22.8 kg/kmol
Density, ρ	1357 kg/m^3
Heat capacity, c_p	2.41 kJ/kg $\cdot$ K
Thermal expansion coeff.,α	6.04×10^{-4} 1/K
Saturation temperature, T_s	273.15 K
Dynamic viscosity, μ	3.7 mPa $\cdot$ s
Vapour pressure, p_v	$<$ 21 mbar

The propellant is produced by dissolving the solid ADN salt in fuel/water mixture. The dissolution of ADN in the mixture results in a drop in temperature and a slowing down of the process, which can then be speeded up by treating it to a warm water bath [28]. Eventhough many propellants are classified within hazard 1 class explosive materials and have restrictions on transportation, the propellant FLP-106 should not fall into this category due to its very low sensitivity and volatility [27].

The method of ignition and the ignition characteristics of the propellant play an important role in propulsion system design. ADN-blend propellants, which contain water, have a significant ignition delay due to water evaporation. Additionally, a hot surface is required to sustain the propellant decomposition. Wilhelm et al have found that thermal ignition using a glowplug yields a stable flame and an acceptable ignition time for FLP-106 propellant [29]. The glowplug needs to be preheated until it reaches a temperature of 900°C. The combustion temperatures range from 1600°C to 1900°C depending upon the chamber pressure [28, 29]. The temperature at which the ADN decomposition starts is 150°C [30]. The ADN undergoes a complete thermal decomposition before entering the main combustion chamber.

4.2 Feed system

The feed system consists of the storage tanks, valves, flow lines, and the tank pressurization system. The margined propellant mass, $m_{p,mg} = 4.7$ kg for the monopropellant system with an $I_{sp} = 260$ s. Considering the liquid phase density of FLP-106 at room temperature (see Tab. 3), the propellant volume $V_p = 3464\,\text{cm}^3$, which in terms of CubeSat units is ~ 3.5 U.

Since the maximum thrust requirement is low compared to the traditional satellite propulsion systems, a pressure-fed system is utilised. However, since the thrust must be precise and constant, a regulated pressure feed is utilised rather than the classical blowdown system. FLP-106 has low volatility and low sensitivity, thus GN_2 is used as the pressurant. The GN_2 is stored in a small tank and supplied to the main propellant tanks through a pressure regulator and a check valve.

A pressurised propellant tank requires a spherical or a cylindrical shape with hemispherical ends for safety reasons. However, for a 3464 cm^3 tank, the radius of the spherical tank will be approximately 9.45 cm, which cannot be accommodated easily in a 16U CubeSat. To minimise the tank volume while main-

taining the pressure and accommodating within the structure, cylindrical tanks with ends containing elliptical dome shapes have to be developed. Since one large tank would be infeasible, four tanks with 980 cm^3 capacity each, including a $\sim 13\%$ ullage volume, are utilised. Each tank has a radius of 4.7 cm and a height of 16.4 cm. The tanks shape and the placement inside the spacecraft structure are illustrated in Fig. 5. Each tank occupies $\sim$ 1.6U space.

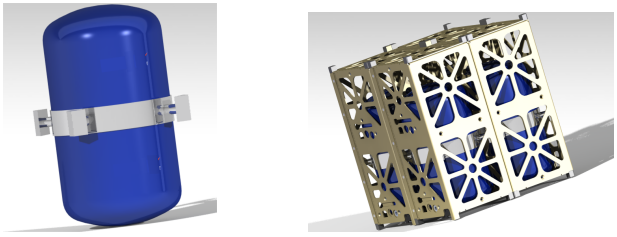

(a) Tank shape **(b)** Full structure

Fig. 5: Tank shape and placement in the spacecraft structure

The feed pressure is set at 2.2 MPa and this yields a Maximum Expected Operational Pressure (MEOP) of 2.6 MPa [31]. The feed pressure value is similar to the one for a high-performance ADN-based monopropulsion system on-board PRISMA satellite. The thickness of the tank wall is determined for a burst pressure of 3.9 MPa, which considers a burst factor of 1.5 applied on MEOP.

The material used for the tank is Titanium alloy Ti-6Al-4V [‡] which has an yield strength of 880 MPa and an ultimate strength of 950 MPa. It is widely used as an implant material and has a very high corrosion resistance. The density of the material is 4430 kg/m^3. The propellant FLP-106 is also compatible with this material [27]. The tank wall thickness is calculated to be 0.2 mm. Laser-assisted machining and other precision techniques applied on Ti-6Al-4V enable the manufacturing of tanks with small thicknesses [32, 33]. The total mass of all tanks is 0.172 kg. If the a steel alloy material AISI4140 with a density of 7850 kg/m^3 and yield strength of 415 MPa is used, the tank thickness is 0.45 mm and the overall tank mass is 0.68 kg, which is 4 times that of the Ti-alloy.

The pressurant gas (GN_2) pressure is considered to be 28 MPa at 323 K [34]. The nitrogen gas density at these conditions is 257.6 kg/m^3. The pressurant gas volume and mass are calculated based on the feed pressure, 2.2 MPa, and feed temperature, 300 K. The GN_2 tank volume is 415.6 cm^3 and the tank dimensions are $r_{gas,tank} = 4.7$ cm and $h_{gas,tank} = 6$ cm. Utilising the same Titanium alloy material, the gaseous tank thickness is 2.24 mm and the tank mass is 0.18 kg. The gas tank occupies $\sim$ 0.6U space in the spacecraft. The feed system design characteristics are listed in Tab. 4. The feed system mass does not include the propellant mass but includes the pressurant gas mass.

Tab. 4: Monopropellant thruster feed system design parameters

Property	**Value**
Propellant tanks	4
Individual tank volume, V_{tank}	980 cm^3
Prop. feed pressure, P_{prop}	2.2 MPa
Prop. tank burst pressure, $P_{prop,burst}$	3.9 MPa
Prop. tank radius, $r_{prop,tank}$	4.7 cm
Prop. tank height, $h_{prop,tank}$	16.4 cm
Prop. tank thickness, th_{prop}	0.2 mm
Total tank mass, m_{tank}	0.172 kg
Press. gas pressure, P_{gas}	28 MPa
Press. gas mass, m_{gas}	0.107 kg
Press. tank volume, $V_{gas,tank}$	415.6 cm^3
Press. tank radius, $r_{gas,tank}$	4.7 cm
Press. tank height, $h_{gas,tank}$	6 cm
Press. tank thickness, $th_{gas,tank}$	2.24 mm
Press. tank mass, $m_{gas,tank}$	0.18 kg
Feed pipes & valves mass, m_{fv}	0.2 kg
Feed system total mass, m_{feed}	0.66 kg
Feed system total volume	7U

4.3 Thruster design and performance

Some studies utilise a hot catalytic bed for the decomposition of ADN [35]. FLP-106 ignites at 200°C temperature [27, 29]. The catalyst bed design is a complicated process and it has not been addressed in this work. In addition to catalystic decomposition and ignition of ADN-based propellants, thermal ignition using a glow-plug and ignition using electrical resistive heating are also functional [29, 30]. In thermal ignition technique, the glow-plug is supplied with power for preheating and sustenance of the hot surface at 900°C. The FLP-106 propellant makes contact with the surface and ignition is initiated. Since a complete ADN decomposition is assumed, the thermal decomposition reaction efficiency $\eta_r = 1$.

The chamber pressure is 2 MPa and the combustion temperature is 1880 K [28, 24]. The specific heat ratio of the combustion products $k = 1.15$ and the

[‡]http://asm.matweb.com/search/SpecificMaterial.asp?bassnum=mtp641

specific gas constant $R_{gas} = 364.7$ J/kg · K, which is calculated using the Molecular Mass $\mathfrak{M} = 22.8$ kg/kmol. The nozzle throat diameter, D_t, is set at 0.5 mm and the effect of the nozzle area ratio on the performance is analysed by varying it from $\varepsilon = 50$ to $\varepsilon = 100$. The nozzle exit pressure, P_e, is determined using the Eq. 6 [36].

$$\frac{A_t}{A_e} = \left(\frac{k+1}{2}\right)^{1/(k-1)} \cdot \left(\frac{P_e}{P_c}\right)^{1/k} \cdot \sqrt{\left(\frac{k+1}{k-1}\right) \cdot \left(1 - \left(\frac{P_e}{P_c}\right)^{(k-1)/k}\right)} \quad (6)$$

Here, A_e and A_t are the nozzle exit and throat areas, respectively. The nozzle is assumed to be a supersonic convergent-divergent conical nozzle and the Mach number at the throat is 1. The mass flow rate $\dot{m}$, the coefficient of thrust C_F, and the characteristic velocity c^* are calculated using Eqs. 7,8 and 9, which are ideal rocket relations. Since the thruster operation occurs in near vacuum conditions, P_{vac} is set as 0.

$$\dot{m} = \frac{A_t \cdot P_c \cdot k}{\sqrt{(k \cdot R_{gas} \cdot T_c)}} \cdot \sqrt{\left(\frac{2}{k+1}\right)^{\frac{k+1}{k-1}}} \quad (7)$$

$$C_{F,ideal} = \sqrt{\frac{2 \cdot k^2}{k-1} \cdot \left(\frac{2}{k+1}\right)^{\frac{k+1}{k-1}} \cdot \left(1 - \left(\frac{P_e}{P_c}\right)^{\frac{k-1}{k}}\right)} + \left(\frac{P_e - P_{vac}}{P_c}\right) \cdot \left(\frac{A_e}{A_t}\right) \quad (8)$$

$$c^*_{ideal} = \frac{1}{k} \cdot \sqrt{k \cdot R_{gas} \cdot T_c \cdot \left(\frac{k+1}{2}\right)^{\frac{k+1}{k-1}}} \quad (9)$$

The nozzle efficiency η_n is assumed to be 0.97 and the reaction efficiency is set at 1 since there is complete decomposition. Thus, the corrected values become,

$$C_{F,corr} = C_{F,ideal} \cdot \eta_n \quad (10)$$

$$c^*_{corr} = c^*_{ideal} \cdot \eta_r \quad (11)$$

Utilising Eqs.7-11, the thrust and specific impulse are calculated using Eqs.12 and 13.

$$T = \dot{m} \cdot c^*_{corr} \cdot C_{F,corr} \quad (12)$$

$$I_{sp} = C_{F,corr} \cdot \frac{c^*_{corr}}{g_0} \quad (13)$$

Considering one thruster, for $\varepsilon = 50$, $P_c = 2$ MPa, $T_c = 1880$ K, and $D_t = 0.5$ mm, the performance values are $\dot{m} = 0.606$ g/s, $C_{F,ideal} = 1.964$, $c^*_{ideal} = 1296$ m/s, $T_{ideal} = 1.542$ N, and $I_{sp,ideal} = 259.5$ s. With $\eta_n = 0.97$, the corrected and estimated performance values are $C_F = 1.905$, $T = 1.496$ N and the $I_{sp} = 251.7$ s. Since two thrusters are used, system is capable of providing $T_{max,ideal} = 3.18$ N, with an estimated $T_{max} = 2.992$ N considering the nozzle efficiency. The thrust and the specific impulse increase with the increase in area ratio, as illustrated in Fig. 6. At $\varepsilon = 100$, $T_{ideal} = 1.591$ N and $I_{sp,ideal} = 267.7$ s, and the $T = 1.543$ N and $I_{sp} = 259.7$ s. The final value of $\varepsilon = 100$ is chosen for the design.

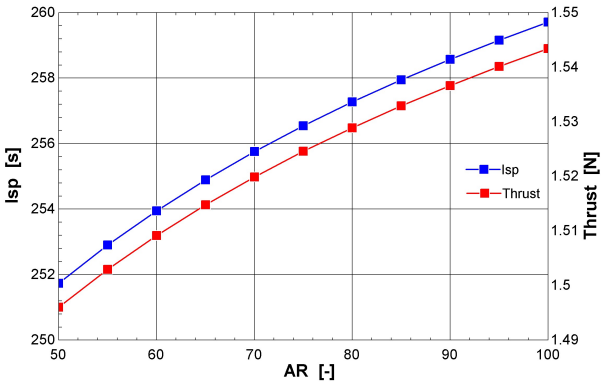

Fig. 6: I_{sp} and T variation with Area Ratio for the monopropellant thruster with $\eta_n = 0.97$

The thruster design parameters such as chamber volume V_c and chamber length L_c are calculated using the desired residence time t_s (see Eqs. 14- 15). The desired residence time t_s is set at 0.001 s to account for ignition and decomposition. The contraction ratio of the nozzle is set at 50 and the chamber diameter D_c is calculated to be 10 $\times D_t$. The nozzle constriction length L_{con} is set as 1.5 mm as a preliminary design choice so as to adjust the constriction half angle to 45°.

$$V_c = t_s \cdot A_t \sqrt{k \cdot R_{gas} \cdot T_c} \cdot \left(\frac{2}{k+1}\right)^{1/(k-1)} \quad (14)$$

$$V_c = A_c \cdot L_c + A_c \cdot L_{con} \cdot \left(1 + \sqrt{\frac{A_t}{A_c}} + \frac{A_t}{A_c}\right) \quad (15)$$

For the set input parameters, the $V_c = 215.3$ mm^3 with $L_c = 9.223$ mm. The A_c and A_t are chamber and throat cross section areas, respectively.

A conical nozzle with a half angle $\alpha = 15°$, $\varepsilon = 100$, and the throat longitudinal radius is set at $1.5 \times R_t$. The length of the divergent part of the nozzle is determined to be $L_N = 8.45$ mm. The chamber and nozzle design parameters are listed in Tab. 5 and the overall performance and system design parameters are listed in Tab. 6. The thrusters are placed outside the 16U spacecraft structure.

Tab. 5: Monopropellant thruster chamber & nozzle design parameters

Property	Value
Thrusters	2
Chamber pressure, P_c	2 MPa
Chamber temperature, T_c	1880 K
Chamber volume, V_c	215.3 mm^3
Chamber diameter, D_c	5 mm
Chamber residence time, t_s	0.001 s
Chamber length, L_c	9.223 mm
Expansion area ratio, ε	100
Expansion half angle, α	15°
Nozzle length (divergent), L_N	8.45 mm
Igniter mass, m_{ig}	0.02 kg
Thruster mass, $m_{thruster}$	0.2 kg

Tab. 6: Monopropellant thruster overall performance and design parameters

Property	Value
Decomposition efficiency, η_r	1
Nozzle efficiency, η_n	0.97
Max Thrust (per thruster)	1.543 N
Specific Impulse, I_{sp}	259.7 s
Exhaust velocity, v_e	2548 m/s
Characteristic velocity, c^*	1296 m/s
Thrust coefficient, C_F	1.905
Mass flow rate (per thruster), $\dot{m}$	0.606 g/s
Max temperature, T_{max}	1880 K
Overall Mass, m_{tot}	5.6 kg

5. Bipropellant thruster

The parametric analysis to find the thrust and burn duration values based on minimum transfer time to escape Earth is performed again for the bipropellant thruster system with an $I_{sp} = 315$ s. The sampled thrusts are between 2 N and 3 N. For the constant burntime strategy, the values of t_b range from 400 to 600 seconds while for the constant burn arc strategy, the values of $\Delta\theta_b$ range from 35° to 55°. For each combination, the trajectory is simulated and the total transfer time is predicted.

The transfer time as a function of T and t_b is illustrated in Fig. 7 and similarly, Fig. illustrates the transfer time as a function of T and $\Delta\theta_b$. The combinations are selected based on the lowest transfer time to escape. The combinations that yield a total transfer time greater than 3600 hours are discarded.

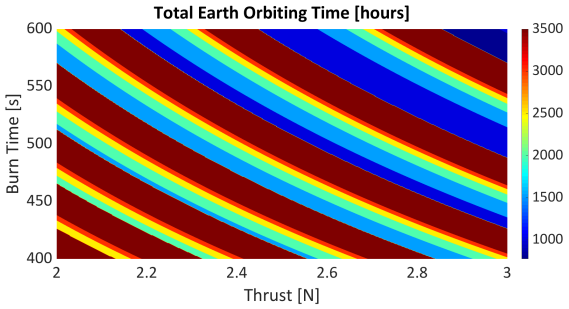

(a) Transfer time (hr) for constant t_b strategy

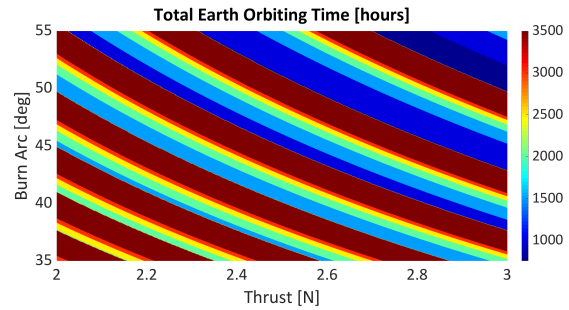

(b) Transfer time (hr) for constant $\Delta\theta_b$ strategy

Fig. 7: Transfer time (hr) as a function of T & t_b and T & $\Delta\theta_b$ for $I_{sp} = 315$ s

The constant burntime strategy yields a combination of $T = 2.882$ N and $t_b = 594.39$ s for each manoeuvre. The shortest total transfer time $P = 774.47$ hours. The maximum and minimum burn arcs during the transfer are 53.6° and 52.40°, respectively. The constant burn arc strategy yields a combination of $T = 2.738$ N and $\Delta\theta_b = 54.9°$. The total transfer time $P = 767.36$ hours. The corresponding maximum and minimum burntimes are 626.24 s and 390.67 s. Manoeuvring at a maximum thrust of 3 N, the t_b becomes 570.51 s, which is a ∼4% decrease and the transfer time increases by $< 1\%$. For the constant burn arc strategy, the $\Delta\theta_b$ becomes 50.3°, which is an 8.3% decrease. Similar to the monopropellant thruster, the bipropellant thruster is also sized for the maximum thrust.

For a propulsion system with $I_{sp} = 315$, the total ΔV for Earth escape is 361.31 m/s and the corresponding propellant mass, $m_p = 3.31$ kg. The spacecraft escapes after 6 manoeuvres and this ΔV is accumulated over these manoeuvres. The ΔV varies from the ideal perigee escape ΔV, 359.66 m/s, by 1% and accounts for the gravity losses. The propulsion system is sized for a margined ΔV_{mg} of 445 m/s, which includes the margined velocity increment to escape, $\Delta V_{mg} = 396$ m/s and the margined circularisation $\Delta V_{circ} = 49$ m/S. The propellant mass, $m_{p,mg}$, corresponding to ΔV_{mg} is 3.61 kg and the propellant mass for circularisation is 0.30 kg. Thus, the overall propellant mass $m_{p,mg,ovr} = 3.91$ kg. A single thruster providing a 3 N thrust is considered. The orbit raising parameters using bipropellant thruster with constant t_b strategy are listed in Tab. 7.

Tab. 7: Orbit raising parameters using bipropellant thruster with constant t_b strategy

Parameter	**Value**
Initial Mass, m_i	30 kg
Required Thrust, T	2.882 N
Specific Impulse, I_{sp}	315 s
Burn Time per manoeuvre, t_b	594.39 s
Orbit raising manoeuvres	6
Ideal ΔV	359.66 m/s
Real ΔV	361.31 m/s
Margined ΔV (10% margin)	396 m/s
Propellant mass (real), m_p	3.31 kg
Propellant mass (margined), $m_{p,mg}$	3.61 kg
Final mass at Earth escape, $m_{f,esc}$	26.39 kg
Margined $\Delta V_{circ,mg}$ ($\sim$10% margin)	49 m/s
Propellant mass for $\Delta V_{circ,mg}$	0.30 kg
Overall propellant mass, $m_{p,mg,ovr}$	3.91 kg

5.1 Propellant properties

Bipropellant thrusters utilising ethanol and hydrogen peroxide for small spacecraft applications have been under development recently [15, 37]. The fuel, ethanol, has a density of 789.3 kg/m^3, molar mass of 49.07 kg/kmol, and a vapour pressure of 5.95 kPa at 293 K. Ethanol freezes at 159 K and vapourises at 351 K.

The oxidiser is a concentrated hydrogen peroxide solution or "high-test peroxide" (HTP) which is 95% w/w H_2O_2 in water. Although H_2O_2 solution is non-flammable and stable when stored properly[38], it readily decomposes into a high temperature ($\sim$ 700°C) mixture of steam and oxygen in contact with a catalyst. The 95% H_2O_2 solution has a density of 1420 kg/m^3 at 293 K. The solution has a molar mass of 33.21 kg/kmol with pure H_2O_2 having 34.01 kg/kmol. The melting point is 272.7 K and the boiling point is 423.35 K.

Both propellants satisfy the requirement CPROP-05 regarding non-toxic propellant usage. However care must be taken while handling highly concentrated H_2O_2 since a skin contact might lead to extensive burns. Additionally, only a few materials are compatible with HTP for long term storage [38]. The metallic or alloy based storage tank material almost always require passivation and conditioning before use. The Titanium alloy (Ti-6Al-4V) and stainless steel coated with Polytetrafluoroethylene (PTFE) are compatible with HTP [38].

5.2 Feed System

The bipropellant feed system contains separate storage tanks for ethanol and H_2O_2. The system also includes a GN_2 tank for propellant pressurisation and separate flow lines and flow control valves. The margined propellant mass $m_{p,mg} = 3.91$ kg for $I_{sp} = 315$ s, which includes the propellant masses for providing the required ΔV for Earth escape and Mars circularisation.

The feed pressure is set at 1.8 MPa and the combustion chamber pressure is assumed to be 1.5 MPa [39]. The mass mixture ratio (O/F) is fixed at 4.5 to ensure a fuel-rich condition during combustion since the vacuum specific impulse $I_{sp,vac}$ is near the maximum value. Eventhough O/F = 4.4 yields the highest I_{sp}, O/F 4.5 is chosen to reduce the heat release while obtaining a similar performance. Fig. 8 represents the I_{sp} and T variation with the O/F ratio and Fig. 9 represents the combustion temperature with the O/F ratio.

The fuel mass, $m_{fuel} = 0.711$ kg and the oxidiser mass m_{ox} 3.199 kg. Considering the densities of the propellants at 293 K, the volumes of fuel and oxidiser are $V_{fuel} = 901$ cm^3 and $V_{ox} = 2253$ cm^3, respectively. Following the same principles to accommodate the propellant tanks in the structure, the fuel is stored in one 1018 cm^3 dome shaped cylindrical tank and the oxidiser is stored in three 848.6 cm^3 tanks, each with 13% ullage volume. Each tank has a radius of 4.7 cm. The height of the fuel tank $h_{fuel,tank} = 17$ cm, occupying 1.7U space. The height of each oxidiser tank $h_{ox,tank} = 14.3$ cm and it occupies $\sim$ 1.4U.

With the feed pressure at 1.8 MPa and the GN_2 pressurant is set at 28 MPa at 323 K [34]. The required GN_2 mass to pressurise all tanks is 0.085 kg.

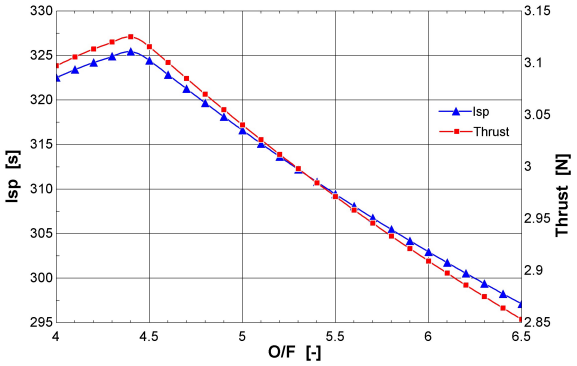

Fig. 8: Theoretical I_{sp} and T variation with O/F; $P_c = 1.5$ MPa, $\varepsilon = 100$, $D_t = 1.15$ mm

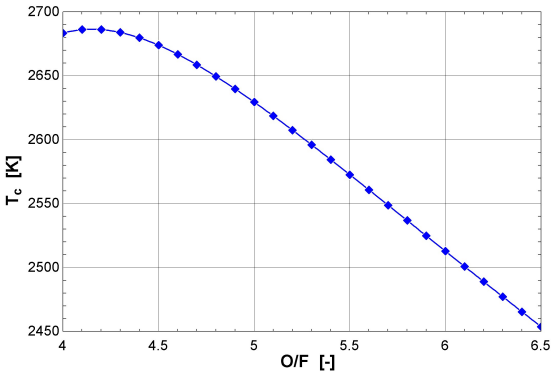

Fig. 9: Combustion Temperature variation with O/F; $P_c = 1.5$ MPa

The GN_2 tank has a volume of 329.5 cm^3, with a radius of 4.7 cm and a height of 5.45 cm, occupying ∼0.5U space. The tank material used is Ti-6Al-4V alloy. The tank MEOP is 2.16 MPa and the tank burst pressure is 3.24 MPa. The thickness of each tank is 0.173 mm. The fuel tank mass $m_{fuel,tank} = 0.0333$ kg and the combined oxidiser tank mass $m_{ox,tank} = 0.0832$ kg. The GN_2 dome shaped tank thickness is 2.24 mm and the corresponding mass $m_{gas,tank} = 0.143$ kg. The feed system characteristics are listed in Tab. 8.

5.3 Thruster design and performance

The high-test peroxide (HTP) or the 95% H_2O_2 solution undergoes an exothermic decomposition when in contact with a catalyst. The resulting vapour readily ignites in contact with a fuel depending upon the conditions in the combustion chamber. The catalyst is placed in a small catalytic chamber outside the main thrust chamber and HTP is fed through. The chosen catalyst is composed of a Cordierite substrate with Platinum Oxide washcoating, where Pt remains as active phase [37]. Although auto-ignition takes place, an electrical spark igniter is placed to ensure proper ignition.

Tab. 8: Bipropellant thruster feed system design parameters

Property	Value
Fuel tanks	1
Oxidiser tanks	3
Fuel tank volume, $V_{fuel,tank}$	1018 cm^3
Ox. tank volume, $V_{ox,tank}$	848.6 cm^3
Feed pressure, P_{prop}	1.8 MPa
Tank burst pressure, $P_{prop,burst}$	3.24 MPa
Tank radius, $r_{prop,tank}$	4.7 cm
Fuel tank height, $h_{fuel,tank}$	17 cm
Ox. tank height, $h_{ox,tank}$	14.3 cm
Tank thickness, th_{prop}	0.173 mm
Fuel tank mass, $m_{fuel,tank}$	0.0333 kg
Ox. tank mass (total), $m_{ox,tank}$	0.0832 kg
Press. gas pressure, P_{gas}	28 MPa
Press. gas mass, m_{gas}	0.163 kg
Press. tank volume, $V_{gas,tank}$	329.5 cm^3
Press. tank radius, $r_{gas,tank}$	4.7 cm
Press. tank height, $h_{gas,tank}$	5.45 cm
Press. tank thickness, $th_{gas,tank}$	2.24 mm
Press. tank mass, $m_{gas,tank}$	0.143 kg
Feed pipes & valves mass, m_{fv}	0.2 kg
Feed system total mass, m_{feed}	0.622 kg
Feed system total volume	6.5 U

At $P_c = 1.5$ MPa, the combustion of ethanol and 95% H_2O_2 yields a combustion temperature $T_c = 2673.9$ K. The specific heat ratio $k = 1.139$ and the combustion gas constant $R_{gas} = 381$ J/kg · K. The nozzle area ratio is set at $\varepsilon = 100$ and the throat diameter is set at $D_t = 1.15$ mm. The resulting mass flow rate $\dot{m} = 0.9792$ g/s. The ideal performance parameters are $C_{F,ideal} = 1.999$, $c^*_{ideal} = 1590.96$ m/s, $v_{e,ideal} = 3181.78$ m/s, $T_{ideal} = 3.114$ N and $I_{sp,ideal} = 324.45$ s. Rocket Propulsion Analysis tool developed by Ponomarenko et al has been utilised to calculate the reaction and nozzle efficiencies as well as the estimated delivered performance of the thruster [40]. The Ethanol-HTP (both at 293 K) reaction efficiency $\eta_r = 0.9612$, the nozzle efficiency $\eta_n = 0.9721$, and the total efficiency $\eta_t = 0.9344$. The corrected performance values are, $C_F = 1.944$, $c^* = 1529.25$ m/s, $v_e = 2972.92$ m/s, $T = 2.911$ N and $I_{sp} = 303.15$ s.

Considering the estimated performance, the propellant mass required for escape increases by 0.12 kg. The variation of T and I_{sp} with the area ratio for the bipropellant thruster is illustrated in Fig. 10.

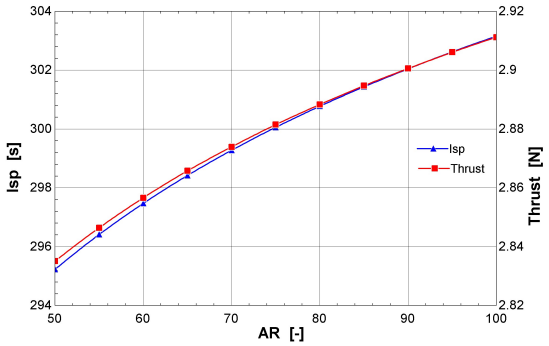

Fig. 10: Estimated I_{sp} and T variation with Area Ratio for the bipropellant thruster; $A_t = 1.039$ mm^2, $P_c = 1.5$ MPa, $\eta_{tot} = 0.9344$

The nozzle contraction ratio is set at 50 and the chamber diameter D_c is calculated to be 8.132 mm, which is ∼7 times larger than D_t. A characteristic length (L^*) of 1.78 m is chosen for the preliminary thruster design [41, 42]. The $L^* = 1.78$ m corresponds to H_2O_2-RP1 combination including the catalyst bed and has been utilised in this case since the value for H_2O_2-Ethanol could not be found. The corresponding residence time $t_s = 0.00268$ s. The nozzle constriction length is set at $L_c = 1.6$ mm. The resulting combustion chamber volume $V_c = 1849$ mm^3 and the combustion chamber length $L_c = 33.74$ mm. With an expansion half angle $\alpha = 15°$ and the throat longitudinal radius is set at $0.75 \times D_t$ [41]. The length of the divergent part of the nozzle $L_N = 19.43$ mm for $\varepsilon = 100$. The chamber and nozzle design parameters are listed in Tab. 9 and the performance parameters are listed in Tab. 10.

The thrust chamber material selection is critically important since the combustion temperature is very high. Niobium alloy is a good candidate since it has a melting temperature of 2741 K and a density of 8570 kg/m^3. The melting temperature is marginally higher than the combustion temperature 2673.9 K. However, the safe operating temperature of the material is 1500 K and a fuel film cooling technique must be utilised to prevent overheating and structural failure [39, 43]. Injecting a coolant at the location of the main fuel injector ensures high cooling capacity and simplicity in design [39].

Tab. 9: Bipropellant thruster chamber & nozzle design parameters

Property	Value
Chamber pressure, P_c	1.5 MPa
Chamber temperature, T_c	2673.9 K
Chamber volume, V_c	1849 mm^3
Chamber diameter, D_c	8.132 mm
Characteristic length, L^*	1.78 m
Chamber residence time, t_s	0.00268 s
Chamber length, L_c	33.74 mm
Expansion area ratio, ε	100
Expansion half angle, α	15°
Nozzle length (divergent), L_N	19.42 mm
Catalytic chamber mass, m_{cat}	0.02 kg
Thruster mass, $m_{thruster}$	0.3 kg

Tab. 10: Bipropellant thruster overall performance and design parameters

Property	Value
Reaction efficiency, η_r	0.9612
Nozzle efficiency, η_n	0.9721
Max Thrust (per thruster)	2.911 N
Specific Impulse, I_{sp}	303.15 s
Exhaust velocity, v_e	2972.92 m/s
Characteristic velocity, c^*	1529.25 m/s
Thrust coefficient, C_F	1.9441
Mass flow rate, $\dot{m}$	0.9792 g/s
Max temperature, T_{max}	2673.9 K
Overall Mass, m_{tot}	4.852 kg

6. Conclusion

This work set out to design and characterise chemical propulsion systems that shall enable a stand-alone interplanetary CubeSat to escape Earth while minimising gravity losses, Van Allen belt crossings, and irrecoverable destabilisation.

A mission analysis was performed to calculate the necessary ΔV for escape while considering finite burn manoeuvres. The required thrust and burn duration combinations were calculated to achieve Earth escape in the shortest time while adhering to system constraints.

Monopropellant thruster design using FLP-106 propellant was pursued and the system was sized using the ΔV requirements. The propellant properties were analysed, the operating pressures were set and the corresponding feed system design characteristics were obtained. The thruster design and performance

calculations were done and a total maximum thrust of 3.18 N (1.54 N each) and an I_{sp} of 259.7 seconds were obtained. The overall system mass was estimated to be 5.6 kg while occupying 7U space in the 16U spacecraft.

A similar design for the bipropellant thruster using Ethanol and H_2O_2 was pursued and the corresponding propellant masses with an O/F ratio of 4.5 was obtained. Catalytic decomposition of H_2O_2 is used to generate the vapours that will readily ignite with the fuel. The performance analysis yielded a maximum thrust of 2.91 N and a I_{sp} of 303.15 s. The system weighs 4.85 kg while occupying 6.5U space.

Both systems require precise control methodologies to tune the thrust and burn duration so as to achieve escape within the shortest time. The systems satisfied the system mass requirement ($< 25\%$) as the monopropellant system weighs 18.7% and the bipropellant system weighs 16.17% of the overall spacecraft mass (30 kg). The performances and the design characteristics of the propulsion systems render the Earth escape and the Mars circularisation using a stand-alone interplanetary CubeSat feasible.

References

[1] T. H. Zurbuchen, R. von Steiger, S. Bartalev, X. Dong, M. Falanga, R. Fléron, A. Gregorio, T. S. Horbury, D. Klumpar, M. Küppers, *et al.*, "Performing high-quality science on cubesats," *Space Research Today*, vol. 196, pp. 11–30, 2016.

[2] F. Topputo, M. Massari, J. Biggs, P. Di Lizia, D. Dei Tos, K. Mani, S. Ceccherini, V. Franzese, A. Cervone, P. Sundaramoorthy, *et al.*, "LUMIO: a cubesat at Earth-Moon L2," in *4S Symposium*, pp. 1–15, 2018.

[3] K. Lemmer, "Propulsion for cubesats," *Acta Astronautica*, vol. 134, pp. 231–243, 2017.

[4] G. Manzoni, "Design of a highly integrated micropropulsion system for microsatellites attitude control," in *36th AIAA/ASME/SAE/ASEE Joint Propulsion Conference and Exhibit*, p. 3476, 2000.

[5] S. S. Board, N. R. Council, *et al.*, *Assessment of Mars science and mission priorities*. National Academies Press, 2003.

[6] S. Asmar and S. Matousek, "Mars Cube One (MarCO): the first planetary cubesat mission," in *Proceedings of the Mars CubeSat/NanoSat Workshop, Pasadena, California, November*, vol. 20, p. 21, 2014.

[7] W. K.-F. Tai, "Mars communication network design trade study," Master's thesis, San Jose State University, 1998.

[8] R. Staehle, D. Blaney, H. Hemmati, M. Lo, P. Mouroulis, P. Pingree, T. Wilson, J. Puig-Suari, A. Williams, B. Betts, *et al.*, "Interplanetary cubesats: opening the solar system to a broad community at lower cost," *Journal of small satellites*, vol. 2, no. 1, pp. 161–186, 2013.

[9] K. Mani, F. Topputo, and A. Cervone, "Dual chemical-electric propulsion systems design for interplanetary cubesats," in *6th Space Propulsion Conference*, pp. 1–12, 2018.

[10] A. Klesh and J. Krajewski, "MarCO: CubeSats to Mars in 2016," in *Proceedings of the 29th Annual AIAA/USU Small Satellite Conference: SSC15-III-3*, 2015.

[11] J. Cardin, K. Coste, D. Williamson, and P. Gloyer, "A cold gas micro-propulsion system for cubesats," in *17th Annual AIAA/USU Conference on Small Satellites*, 2003.

[12] R. Walker, D. Kochny, C. Bramanti, and I. Carnelli, "Miniaturised Asteroid Remote Geophysical Observer (M-ARGO): a stand-alone deep space cubesat system for low-cost science and exploration missions," in *6th Interplanetary CubeSat Workshop - Cambridge*, iCubeSat, 2017.

[13] C. Scharlemann, M. Schiebl, K. Marhold, M. Tajmar, P. Miotti, C. Kappenstein, Y. Batonneau, R. Brahmi, and C. Hunter, "Development and test of a miniature hydrogen peroxide monopropellant thruster," in *42nd AIAA/ASME/SAE/ASEE Joint Propulsion Conference & Exhibit*, p. 4550, 2006.

[14] D. Scharfe and A. Ketsdever, "A review of high thrust, high delta-v options for microsatellite missions," in *45th AIAA/ASME/SAE/ASEE Joint Propulsion Conference & Exhibit*, p. 4824, 2009.

[15] C. Scharlemann and M. Tajmar, "Development of propulsion means for microsatellites," in *43rd AIAA/ASME/SAE/ASEE Joint Propulsion Conference & Exhibit*, p. 5184, 2007.

[16] H. Barber, C. Buell, G. Falkenstein, and R. Gurnitz, "Microthrusters employing catalytically reacted N2-O2-H2 gas mixtures, Tridyne," *Journal of Spacecraft and Rockets*, vol. 8, no. 2, pp. 111–116, 1971.

[17] J. Mueller, R. Hofer, and J. Ziemer, "Survey of propulsion technologies applicable to cubesats," in *Joint Army-Navy-NASA-Air Force (JANNAF), Colorado Springs, CO; United States*, 2010.

[18] M. M. Micci, *Micropropulsion for small spacecraft*, vol. 187. Aiaa, 2000.

[19] B. Reed, W. d, and L. Dang, "Experimental evaluation of cold flow micronozzles," in *37th Joint Propulsion Conference and Exhibit*, p. 3521, 2001.

[20] F. Maggi, G. Gariani, L. Galfetti, and L. T. DeLuca, "Theoretical analysis of hydrides in solid and hybrid

rocket propulsion," *international journal of hydrogen energy*, vol. 37, no. 2, pp. 1760–1769, 2012.

[21] A. Ketsdever and J. Mueller, "Systems considerations and design options for microspacecraft propulsion systems," in *35th Joint Propulsion Conference and Exhibit*, p. 2723, 1999.

[22] F. Topputo and E. Belbruno, "Earth–mars transfers with ballistic capture," *Celestial Mechanics and Dynamical Astronomy*, vol. 121, no. 4, pp. 329–346, 2015.

[23] F. Soler Lanagrán, "Low-thrust heliocentric transfer with ballistic capture and orbit circularization for a standalone mars cubesat," Master's thesis, Politecnico di Milano, 2018.

[24] N. Wingborg and J. de Flon, "Characterization of the ADN-based liquid monopropellant FLP-106," *Space Propulsion 2010*, pp. 3–6, 2010.

[25] A. S. Gohardani, J. Stanojev, A. Demairé, K. Anflo, M. Persson, N. Wingborg, and C. Nilsson, "Green space propulsion: Opportunities and prospects," *Progress in Aerospace Sciences*, vol. 71, pp. 128–149, 2014.

[26] K. Anflo and B. Crowe, "In-space demonstration of an ADN-based propulsion system," in *47th AIAA/ASME/SAE/ASEE Joint Propulsion Conference & Exhibit*, p. 5832, 2011.

[27] M. Wurdak, F. Strauss, L. Werling, H. K. Ciezki, D. Greuel, R. Lechler, N. Wingborg, D. Hasan, and C. Scharlemann, "Determination of fluid properties of the green propellant FLP-106 and related material and component testing with regard to applications in space missions," in *Space Propulsion Conference, Bordeaux, France*, 2012.

[28] A. Larsson and N. Wingborg, "Green propellants based on ammonium dinitramide (ADN)," in *Advances in Spacecraft Technologies*, InTech, 2011.

[29] M. Wilhelm, M. Negri, H. Ciezki, and S. Schlechtriem, "Preliminary tests on thermal ignition of ADN-based liquid monopropellants," *Acta Astronautica*, 2018.

[30] N. Wingborg, A. Larsson, M. Elfsberg, and P. Appelgren, "Characterization and ignition of ADN-based liquid monopropellants," in *41st AIAA/ASME/SAE/ASEE Joint Propulsion Conference & Exhibit*, p. 4468, 2005.

[31] K. Anflo and R. Möllerberg, "Flight demonstration of new thruster and green propellant technology on the prisma satellite," *Acta Astronautica*, vol. 65, no. 9-10, pp. 1238–1249, 2009.

[32] C. R. Dandekar, Y. C. Shin, and J. Barnes, "Machinability improvement of titanium alloy (ti–6al–4v) via lam and hybrid machining," *International Journal of Machine Tools and Manufacture*, vol. 50, no. 2, pp. 174–182, 2010.

[33] A. Polishetty, M. Goldberg, G. Littlefair, M. Puttaraju, P. Patil, and A. Kalra, "A preliminary assessment of machinability of titanium alloy ti 6al 4 v during thin wall machining using trochoidal milling," *Procedia Engineering*, vol. 97, pp. 357–364, 2014.

[34] J. R. Wertz, D. F. Everett, and J. J. Puschell, "Space mission engineering: the new smad," ch. 18, pp. 545–546, Microcosm Press, 2011.

[35] M. Negri, M. Wilhelm, C. Hendrich, N. Wingborg, L. Gediminas, L. Adelöw, C. Maleix, P. Chabernaud, R. Brahmi, R. Beauchet, *et al.*, "New technologies for ammonium dinitramide based monopropellant thrusters–The project RHEFORM," *Acta Astronautica*, vol. 143, pp. 105–117, 2018.

[36] G. P. Sutton and O. Biblarz, *Rocket propulsion elements*. John Wiley & Sons, 2010.

[37] A. Woschnak, D. Krejci, M. Schiebl, and C. Scharlemann, "Development of a green bipropellant hydrogen peroxide thruster for attitude control on satellites," *Progress in Propulsion Physics*, vol. 4, pp. 689–706, 2013.

[38] G. Rarata and P. Surmacz, "The safe preparation of HTP and concentrated H2O2 samples," *Prace Instytutu Lotnictwa*, pp. 121–130, 2011.

[39] W. Wieling, B. Zandbergen, A. Mayer, and F. Schretijer, "Development of a hydrogen peroxide/ethanol thruster for the advanced re-entry vehicle," in *3rd Space Propulsion Conference*, 2012.

[40] A. Ponomarenko, "RPA-Tool for Rocket Propulsion Analysis," in *Space Propulsion Conference*, 2014.

[41] B. Zandbergen, "Lecture notes in thermal rocket propulsion," Faculty of Aerospace Engineering, Delft University of Technology, 2010.

[42] D. K. Huzel, *Modern engineering for design of liquid-propellant rocket engines*, vol. 147. AIAA, 1992.

[43] T. E. Tietz and J. W. Wilson, *Behavior and properties of refractory metals*. Edward Arnold, London, 1965.